

Local memory allocation recruits memory ensembles across brain regions

Highlights

- Recruitment of neurons to a memory is coordinated across brain regions
- Memory ensembles recruit presynaptic neurons during learning by a retrograde mechanism
- Higher connectivity between task-specific ensembles improves mice performance

Authors

Ayal Lavi, Megha Sehgal, Andre F. de Sousa, ..., Anna Okabe, Cameron Bear, Alcino J. Silva

Correspondence

silvaa@mednet.ucla.edu

In brief

Lavi et al. show that ensembles of memory neurons in one brain region recruit presynaptic partners in other regions to participate in memory retrieval. We trace brain-wide connectivity between memory ensembles in mice and discover that they are coordinated by a retrograde mechanism.



Report

Local memory allocation recruits memory ensembles across brain regions

Ayal Lavi,¹ Megha Sehgal,¹ Andre F. de Sousa,¹ Donara Ter-Mkrtyan,¹ Fardad Sisan,¹ Alessandro Luchetti,¹ Anna Okabe,¹ Cameron Bear,¹ and Alcino J. Silva^{1,2,*}

¹Departments of Neurobiology, Psychology, Psychiatry, Integrative Center for Learning and Memory and Brain Research Institute, University of California, Los Angeles, Los Angeles, CA, USA

²Lead contact

*Correspondence: silvaa@mednet.ucla.edu

<https://doi.org/10.1016/j.neuron.2022.11.018>

SUMMARY

Memories are thought to be stored in ensembles of neurons across multiple brain regions. However, whether and how these ensembles are coordinated at the time of learning remains largely unknown. Here, we combined CREB-mediated memory allocation with transsynaptic retrograde tracing to demonstrate that the allocation of aversive memories to a group of neurons in one brain region directly affects the allocation of interconnected neurons in upstream brain regions in a behavioral- and brain region-specific manner in mice. Our analysis suggests that this cross-regional recruitment of presynaptic neurons is initiated by downstream memory neurons through a retrograde mechanism. Together with statistical modeling, our results indicate that in addition to the anterograde flow of information between brain regions, the establishment of interconnected, brain-wide memory traces relies on a retrograde mechanism that coordinates memory ensembles at the time of learning.

INTRODUCTION

Memories are stored in sparse populations of neurons in multiple brain regions,^{1–3} and recent studies indicate that neurons participating in memory encoding (sometimes referred to as memory engrams) have stronger connectivity than non-encoding neurons across different regions.^{4,5} However, it remains unknown how these inter-regional connections are coordinated at the time of learning to ensure that all memory ensembles form a coherent pathway that can be readily activated during memory retrieval.

The recruitment of neuronal ensembles to a memory trace in a given brain region is not random, but has been shown to depend on the relative levels of cAMP response element-binding protein (CREB) expression and cellular excitability in individual neurons.^{6,7} This memory allocation mechanism has been observed in multiple brain regions and in different behavioral tasks,^{8–10} suggesting that it is a universal mechanism for memory allocation in the mammalian brain. In conditioned taste aversion (CTA), CREB-mediated memory allocation has been demonstrated in the insular cortex (IC)⁹ and the basolateral amygdala (BLA),⁷ two interconnected regions crucial for CTA memory formation. Because memory depends on neuronal ensembles in multiple brain regions, it raises the question of whether neuronal recruitment is coordinated or independent across regions.

To investigate this question, we developed a novel approach with viral vectors that allows for both the expression of CREB (vCREB) in a sparse population of cells and for the identification of their presynaptic partners in other brain regions during mem-

ory processes. We found that recruitment of neurons for encoding a CTA memory in the BLA and IC follows specific rules, where cells that are selected in one brain region directly recruit their presynaptic partners in the other brain region. Specifically, biasing the recruitment of the memory trace to vCREB neurons in the BLA before learning increases the likelihood that IC neurons presynaptic to those cells are also recruited to the same trace following learning. Likewise, vCREB neurons in the IC directly recruit presynaptic partners in the BLA, suggesting a bidirectional interaction between both brain regions to coordinate the formation of CTA memory trace. This coordination effect was task-specific and was also observed between the BLA and the auditory cortex (AuCtx) during auditory fear conditioning (AFC).

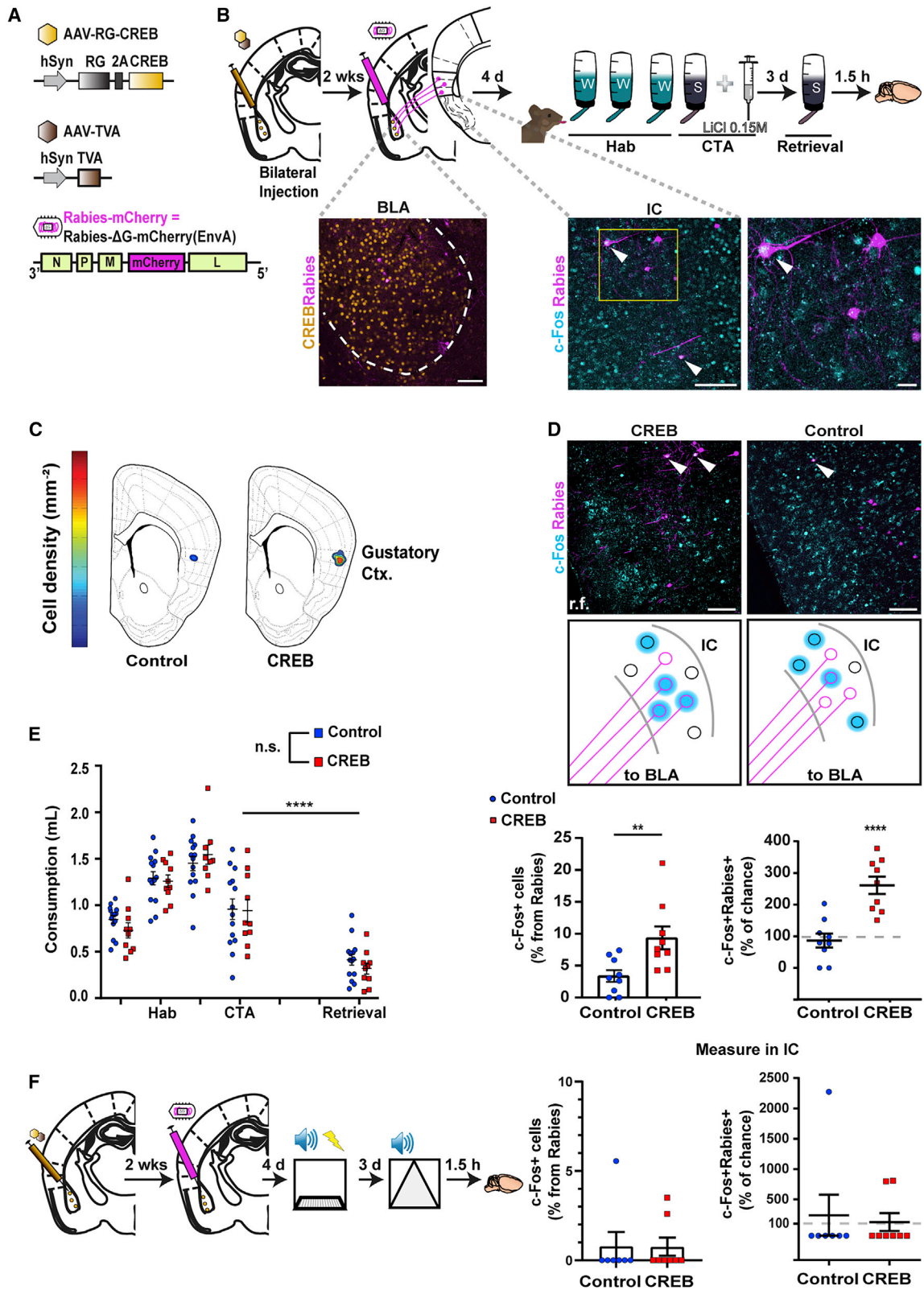
These results, together with statistical modeling, suggest that the formation of a brain-wide memory trace involves the coordination of memory ensembles in relevant brain regions via a retrograde mechanism that is specific to the brain regions involved in the formation of different types of memory.

RESULTS

Memory allocation in BLA during CTA specifically recruits presynaptic neurons in IC

During CTA, temporally precise coordination between BLA and IC is necessary for the formation of a long-term aversive memory.^{11,12} We have previously demonstrated that expression of vCREB in a subset of neurons in either the BLA or IC biases





(legend on next page)

CTA memory allocation to those neurons.^{7,9} Thus, to investigate the possibility of cross-regional coordination between memory ensembles, we developed a novel approach that allocates memory to specific neurons in one brain region (e.g., during CTA) and identify their presynaptic partners in another brain region. This approach, termed cross-regional afferent network of memory ensembles (CRANES; Figure 1A), integrates vCREB with rabies G-protein (RG-CREB; separated by 2A) and TVA receptor expression to allow for the identification of brain-wide presynaptic neurons from vCREB neurons.

Our CRANE method confirmed well-known cortical projections to the BLA (Figures S1A–S1C),^{13–15} including those from the IC, the AuCtx, and the primary motor cortex (M1). As a control, we used a virus expressing the cerulean fluorescent protein (CFP) instead of CREB (RG-CFP) to label a random population of cells in the BLA (see STAR Methods). RG-CREB or RG-CFP viruses were mainly expressed in a small sub-population of BLA neurons (Figures S1D and S1E; 12.2% ± 2.78% RG-CREB, 9.3% ± 1.04% RG-CFP) and retrograde tracing identified similar brain regions in both groups (Figure S1F). As expected,^{7,16,17} RG-CREB-expressing neurons in the BLA biased memory to these neurons which were 2 times more likely to be involved in CTA memory than neighboring cells and chance levels (Figure S1G). Thus, this system allowed testing whether biasing allocation to random neurons in the BLA before learning affects allocation of memory to neurons in other brain regions that are directly connected to RG-CREB neurons in the BLA.

Using the CRANE system in the BLA during CTA and c-Fos immunohistochemistry, we identified IC rabies-positive neurons that were active during memory retrieval (Figure 1B). Contrary to the control group (RG-CFP), the majority of rabies-positive neurons in the experimental group (RG-CREB) were specifically activated in the taste-specialized gustatory IC (but not in IC areas for other sensory modalities)¹⁸, suggesting a high degree of specificity of our system for IC areas relevant for CTA memory (Figure 1C). These IC neurons projecting to BLA RG-CREB neurons were 2.5 times more likely to be activated during memory retrieval in the experimental group than in the control group, or in comparison to chance levels (Figure 1D), and this effect was dependent on NMDA-receptor activity in the BLA (Figures S2B and S2C). Importantly, there was no difference in CTA memory (Figures 1E and S1H–S1J) between groups nor a difference in the percentage of c-Fos or rabies-positive cells throughout the IC (Figures S1K–S1M). In addition to the IC, we also character-

ized active rabies-positive neurons in M1, and in AuCtx, two brain regions that are not involved in CTA,¹⁹ and found no difference between groups or from chance levels (Figure S2A), demonstrating that learning only recruits presynaptic neurons in the brain regions relevant to the specific behavioral task.

To further test behavioral specificity, we repeated the CRANE-BLA experiment except we trained mice in an AFC task. Unlike our results with CTA, our analyses of the activation of rabies-positive IC neurons during AFC memory retrieval revealed no differences between RG-CREB and RG-CFP groups (Figure 1F). Thus, local allocation to RG-CREB neurons in the BLA prior to learning preferentially recruited presynaptic neurons in task-specific regions during CTA. Although RG-CREB expression in the BLA was similar between CTA and AFC, we found a significant increase in the number of rabies-positive neurons in the IC of mice trained in the CTA task when compared with mice trained in the AFC task (CTA 0.95% ± 0.197%, AFC 0.27% ± 0.04%; Figures S2D–S2F). This difference might reflect the known preference of rabies virus to trace active connections between neurons and to highlight experience-dependent changes in connectivity between brain regions.^{20,21}

Altogether these results suggest that memory allocation in the BLA directly recruits presynaptic neurons in particular areas of the IC when this brain region is involved in memory encoding. This suggests that the formation of an inter-regional memory trace may be coordinated via a retrograde mechanism.

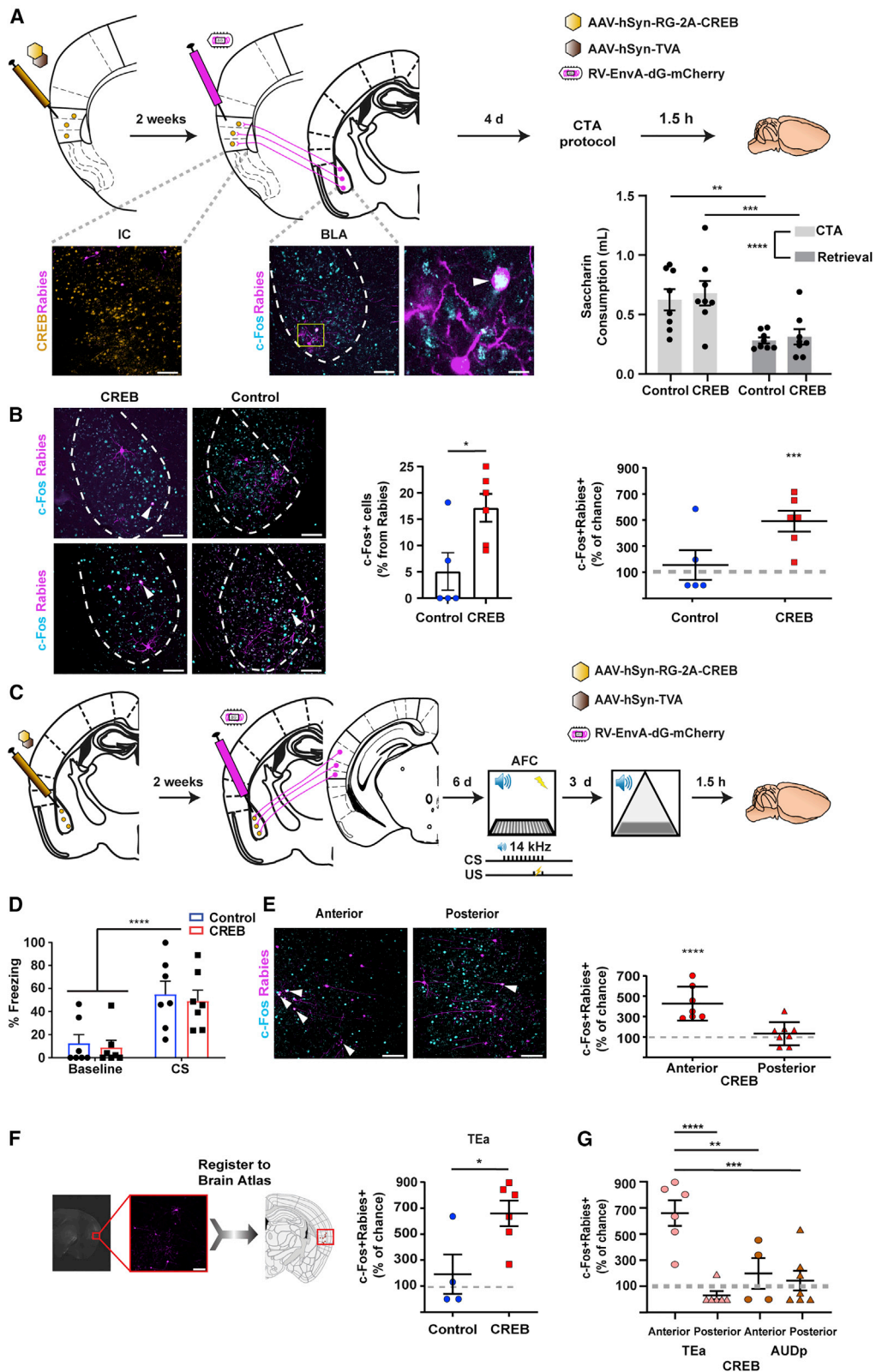
Recruitment of presynaptic memory ensembles during CTA is bidirectional between cortical and sub-cortical regions

Previous studies showed that the connectivity between the BLA and the IC is bidirectional^{13,22,23} and that projections in both directions mediate CTA encoding and retrieval.^{11,24,25} It is possible that the retrograde mechanism that helps to coordinate the recruitment of memory ensembles from the IC to BLA, a sub-cortical region, may also do so for the IC, a cortical region. To test this hypothesis, we applied the CRANE approach described above to manipulate CTA memory allocation in the IC and characterized c-Fos and rabies-related expression in the BLA (Figure 2A).

Our analyses showed that BLA rabies-positive neurons in the CREB group were more likely to be activated during CTA memory retrieval, when compared with the CFP group or with chance levels (Figure 2B). Similar to above, memory retrieval was similar

Figure 1. Memory allocation in BLA during CTA specifically recruits presynaptic neurons in IC.

(A) The CRANE system. RG-CREB and TVA viruses target Rabies-mCherry virus to memory-allocated neurons.
 (B) Experimental design. RG-CREB (orange) or RG-CFP (control) were injected to BLA before CTA. RG-CREB and Rabies-mCherry (magenta) in BLA (left) and in presynaptic IC neurons expressing c-Fos following CTA retrieval (middle). Right: magnified yellow square, arrow indicates co-expression with c-Fos (cyan).
 (C) Both groups learn CTA with no differences during habituation (“Hab”), acquisition (“CTA”), and retrieval (2w-RM ANOVA).
 (D) Higher density (mm^{-2}) of rabies c-Fos-positive neurons in the gustatory IC (“Gustatory Ctx.”) of the CREB group, but not the control group (r.f., rhinal fissure).
 (E) Presynaptic IC neurons projecting to BLA RG-CREB neurons are 2.5 times more likely to co-express c-Fos in comparison to presynaptic IC neurons projecting to BLA RG-CFP neurons. Top: Rabies-mCherry (magenta) and c-Fos (cyan) in IC neurons projecting to RG-CREB BLA neurons or BLA CFP neurons. Middle: higher activation of rabies-positive neurons in the CREB group. Bottom-left: higher c-Fos expression in IC rabies-positive neurons in the CREB group (t test). Bottom-right: c-Fos expression in rabies-positive IC neurons, normalized to chance levels per mouse. CREB group showed increase over chance levels (Fisher’s exact test).
 (F) Task-specific c-Fos expression in rabies-positive IC neurons following AFC. No difference in c-Fos expression between the CREB, control (t test) and also from chance levels (Fisher’s exact test).
 Scale bars, 100 μm (B, 20 μm inset). **p < 0.01, ****p < 0.0001, mean ± SEM.



(legend on next page)

between groups, and the overall percentage of rabies-positive or c-Fos positive cells was not different between the CREB and control (Figures S3A and S3D–S3F). Hence, the retrograde mechanism described above, which coordinates memory allocation through projections from IC to BLA, also has a role in coordinating memory allocation in the projection from the BLA to IC memory ensembles during CTA. As expected, memory was allocated to RG-CREB-expressing neuron on the IC⁹ (Figure S3B), and IC-BLA projections were more abundant than the other direction²³ (Figure S3C).

These findings indicate that the recruitment of presynaptic neurons during memory encoding is not specific to BLA and that it might be a general mechanism that operates across different brain regions.

Recruitment of presynaptic memory ensembles is region- and task-specific

To test whether the mechanism described above also coordinates memory ensembles across other brain regions involved in different forms of learning, we used CRANE in the BLA during AFC (Figure 2C). In addition to the BLA, this behavior engages the AuCtx,^{7,26} which has been shown to monosynaptically project to the BLA.^{4,13,27,28} Both RG-CREB and control showed similar levels of AFC memory (Figures 2D and S4A). Consistent with the role of CREB in AFC memory allocation in the BLA,⁷ RG-CREB neurons in the BLA were 3 times more likely to be activated compared with control neurons during AFC memory retrieval (Figure S4B). We then investigated whether, similarly to the result we obtained for the IC in CTA, presynaptic neurons in the AuCtx, which are connected to RG-CREB neurons in the BLA, are preferentially recruited to the auditory memory trace.

The AuCtx displays a tonotopic map, where specific tones are preferentially activated in different parts of this structure and previous studies^{29,30} suggested that the specific tone used in our studies (14 kHz) is encoded in the anterior AuCtx. Therefore, we analyzed the activation of rabies-positive neurons in the anterior AuCtx of the RG-CREB and found that rabies-positive neurons were more likely to be activated compared with rabies-positive neurons in the posterior AuCtx and chance levels (Figures 2E and S4C). To further investigate regional specificity, we registered the AFC images to a brain atlas³¹ and identified neurons that were both rabies and c-Fos positive (Figure 2F).

Rabies-positive neurons in the temporal association area (TEa) of the ventral AuCtx in the CREB group were 7 times more likely to be activated compared with the control group or chance levels (Figure 2F). This region is not only known to encode the tone we used, it has also been shown to be highly connected to the BLA.^{13,32,30} In contrast, in other regions of the AuCtx, we did not detect differences between the groups and chance levels (Figures 2G and S4D–S4G).

We also quantified the recruitment of presynaptic neurons in the posterior IC (pIC), the interoceptive cortex, a brain region that has been implicated in processing auditory stimuli and fear memory expression.^{30,33,34} We observed no difference between RG-CREB and control group in the activation of rabies-positive neurons, despite a significant increase in the number of c-Fos-positive and rabies-positive neurons in both groups, in comparison to the gustatory IC (Figures S4H–S4J). These results suggest that although pIC projections to the BLA regulate AFC expression,³⁵ memory allocation to specific pIC neurons might not be coordinated by BLA memory ensembles.

Altogether, these results demonstrate that the retrograde mechanism identified above also plays a role in coordinating memory allocation across brain regions for other types of memory suggesting a universal role in recruiting memory allocation across brain regions.

Recruitment of memory ensembles across brain regions supersedes region-specific allocation mechanisms

Thus far, our findings indicate that in addition to allocation mechanisms that act locally within a brain region,^{7–9} there are retrograde mechanisms that operate across brain regions to control the recruitment of presynaptic neurons into memory ensembles (Figures 1 and 2). To understand whether these processes support or interfere with each other in CTA, we used the CRANE system in the BLA, and also expressed vCREB in the IC (Figure 3A). We reasoned that expressing CREB in both the BLA and IC would create two populations of neurons within the IC that could compete for recruitment into memory ensembles in this structure: locally, memory allocation is expected to be biased to vCREB-expressing IC neurons (Figure S4B) and due to the retrograde mechanism described above, RG-CREB expression in BLA neurons should also affect memory allocation in IC neurons (Figure 1E). We found that

Figure 2. Recruitment of presynaptic memory ensembles is bidirectional and task-specific between cortical and sub-cortical regions

(A) Experimental design. RG-CREB (orange) or control RG-CFP was injected in the IC. Rabies-mCherry (magenta) and c-Fos (cyan) in presynaptic BLA neurons projecting to RG-CREB/control neurons in the IC. Middle-right: magnified yellow square, arrow indicates co-expression with c-Fos. Right: same CTA level for CREB/control (n = 7–8).

(B) Rabies-mCherry BLA co-localized with c-Fos. CREB group shows more co-localization between rabies and c-Fos positive cells in the BLA (left, white arrows). Presynaptic BLA neurons projecting to RG-CREB neurons in the IC are 3 times more likely to co-express c-Fos compared with control (middle, n = 5–6, t test) and to chance (right, Fisher's exact test).

(C) AFC experimental design.

(D) Same freezing levels following AFC for CREB/control.

(E) More activated rabies-positive neurons (expressing c-Fos, white arrowheads) in anterior auditory cortex of the CREB group (n = 7–8; t test) and also above chance levels (Fisher's exact test).

(F) Neuroanatomic-based analyses of activated rabies-positive neurons in subregions of the auditory cortex showed more activation (c-Fos) in the temporal association area (TEa) of CREB group (t test) and to chance levels (Fisher's exact test).

(G) In the CREB group, more activated rabies-positive neurons in the anterior TEa in comparison to posterior TEa and primary auditory cortex (AUDp).

Scale bars, 100 μ m (20 μ m inset). t test for (B and D–F). One-way (G) or two-way repeated-measure ANOVA (A), ****p < 0.0001, ***p < 0.001, **p < 0.01, *p < 0.05, mean \pm SEM.

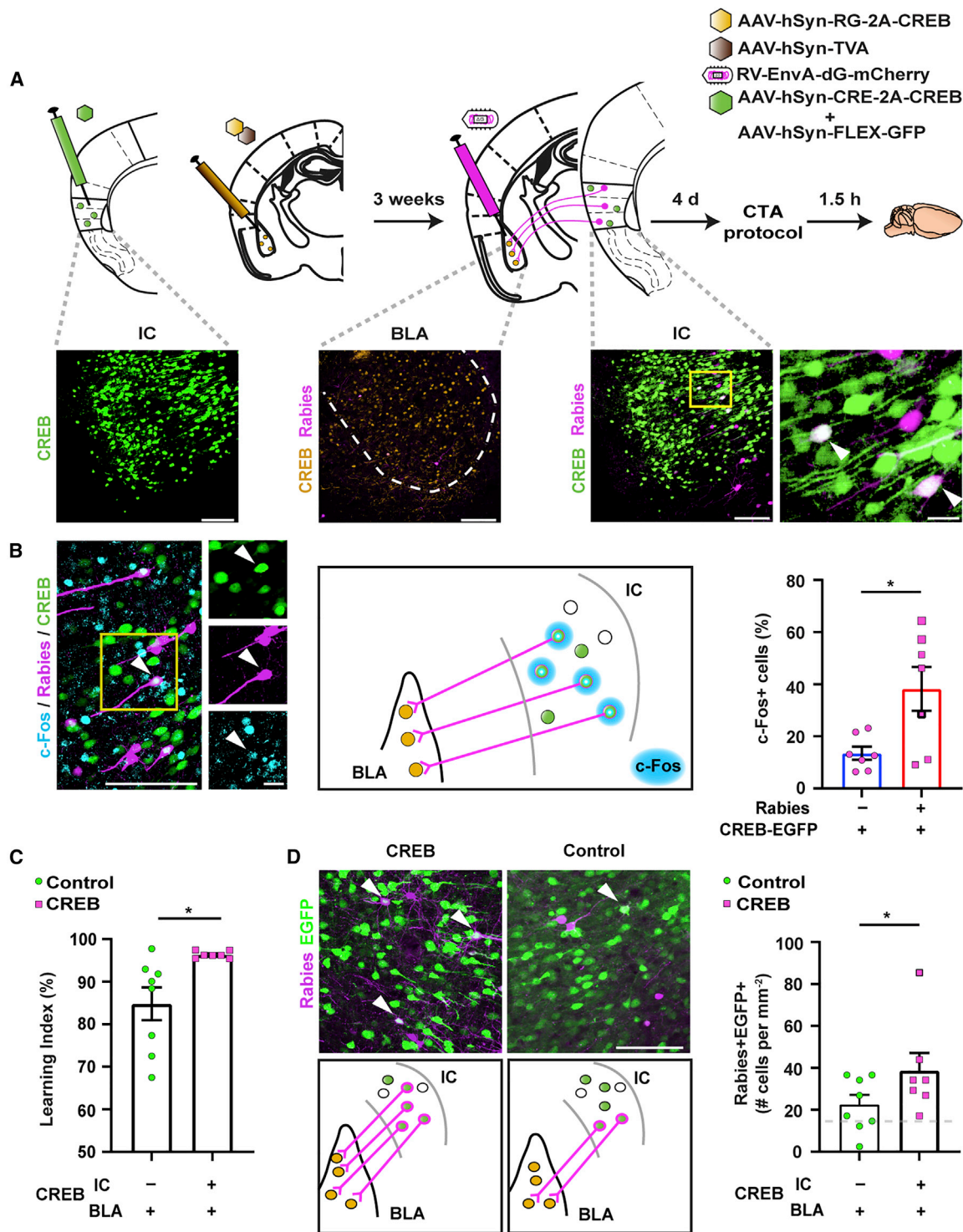


Figure 3. Expression of CREB in the BLA and IC improves CTA memory by enhancing connection probability between BLA and IC memory neurons

(A) In the CREB group, vCREB was injected in the IC (green) in addition to RG-CREB (orange) in the BLA (control = no vCREB in IC). 3 weeks later, Rabies-mCherry (magenta) was infused into the BLA. Middle-right: IC neurons co-expressing Rabies-mCherry and vCREB in the IC. Right: yellow square magnified.

(B) Within the CREB group, BLA-projecting vCREB IC neurons are more likely to be recruited into memory ensembles compared with IC vCREB neurons that do not project to the BLA. Yellow square shows co-expression of vCREB, Rabies-mCherry, and c-Fos (cyan). IC vCREB rabies-positive neurons (EGFP/mCherry/c-Fos-positive) more activated than IC vCREB neurons that do not project to the BLA (EGFP/c-Fos positive, mCherry-negative).

(legend continued on next page)

CREB-positive IC neurons that project to BLA RG-CREB neurons were 2.5 times more likely to be reactivated during memory retrieval than neighboring vCREB-positive neurons and 4 times more likely than neighboring vCREB-negative neurons (Figures 3B and S5A–S5C). These data demonstrate that memory is more likely to be allocated to neurons that are connected to other memory neurons in another structure (i.e., inter-regional memory neurons), in comparison to memory neurons that are not connected to other memory neurons in other structures (i.e., local memory neurons), suggesting that the retrograde recruitment of presynaptic neurons across brain regions supersedes local memory allocation mechanisms.

Enhanced CTA performance is associated with more connected neurons across task-specific brain regions

In the experiment described above, we found that expression of CREB in both the IC and the BLA resulted in enhanced CTA memory, compared with expression only in the BLA (Figures 3C and S1H). Importantly, our analyses showed that CREB expression in both brain regions did not affect the overall levels of rabies, c-Fos, or EGFP-positive neurons, between the CREB (vCREB in IC) and the control group (CFP in IC; Figures S5D–S5F), indicating that the observed difference in behavioral performance may not be due to a larger participation of memory neurons in memory retrieval.

It has previously been suggested that variations in rabies labeling represent changes in input following a task or an experience.²⁰ Therefore, it is possible that the retrograde mechanism described here increased the number of connected vCREB neurons across these two brain regions and that this in turn enhanced CTA memory. Indeed, 3 days after training, we observed an increase in the number of IC vCREB neurons that were also rabies-positive in the CREB group in comparison with the control group, indicating that expression of CREB in both the IC and BLA resulted in more connections between CREB neurons in these two brain regions (Figures 3D and S5G), which was also higher than chance levels (Figure S5H). Hence, expression of vCREB in the IC and BLA organized memory ensembles in these two regions following CTA, such that more vCREB memory ensembles were connected between the IC and BLA, and this in turn may have strengthened memory for CTA (Figures 3C, 3D, and S5I).

A statistical model supports the role of a retrograde mechanism in coordinating the recruitment of memory ensembles across brain regions

The results presented above suggest that a retrograde mechanism has a key role in coordinating the recruitment of memory ensembles across different brain regions. To formally address this hypothesis, we used statistical models of four different possibilities that could account for the formation of memory ensembles in two interacting brain regions (i.e., BLA and IC; Figure 4).

Four key elements were considered in these models: BLA RG-CREB neurons, BLA-IC connectivity, and BLA and IC memory neurons (expressing c-Fos; Figure 4A). We used the data obtained from the literature to generate model predictions and compared these predictions with the data obtained from our results (numbers obtained from our results are consistent with published studies^{7–9}; see STAR Methods).

The anterograde model is based on the premise that BLA neurons that are innervated by IC memory neurons have a higher chance of participating in memory encoding and storage. This idea, which has received tacit support in many neuroscience models,^{36,37} assumes that information from the senses is processed in multiple downstream brain regions and that memory neurons in one region determine which downstream neurons go on to encode and store memory. This model predicts that the percentage of RG-CREB BLA neurons that encode taste information and receive presynaptic projections from IC memory neurons (rabies and c-Fos positive), of all the BLA memory neurons, should be 6% (Figure 4B, middle-right). In contrast, in our experiments, we found that 36% of the BLA memory neurons (c-Fos-positive after retrieval) were RG-CREB positive, 6 times higher than expected, suggesting that the anterograde mechanism alone could not account for our results in the BLA.

In the random co-activation model, the allocation of neurons in the BLA and IC is independent, and there is a chance that memory neurons are connected across regions. This model underestimates the percentage of IC memory neurons that project to BLA memory neurons by 7-fold and thus random co-activation alone could not account for our results in the IC.

The mixed model is based on the hypothesis that allocation from the BLA is coordinated across brain regions only by neurons that both receive and send (evenly distributed) projections to the IC (Figures S1M and S3F). This model predicts that the percentage of IC memory neurons that connect to RG-CREB BLA memory neurons, of all of the IC memory neurons, is 0.0029% (Figure 4B, right), three orders of magnitude lower than experimentally observed data and hence cannot account for our results.

In the retrograde model, memory neurons in the BLA affect the probability that presynaptic neurons in the IC would be engaged in memory encoding and retrieval. This model predicts that the percentage of IC memory neurons that connect to RG-CREB BLA memory neurons, of all of the IC memory neurons, would be 2.22% (Figure 4B, left), which agrees with our experimental findings (3% ± 0.92%; Figure 4B). These results show that the retrograde model best explains the results presented here. Our results suggest a model (Figure 4C) in which memories are allocated to neurons in the BLA and during training, presynaptic neurons in task-relevant brain regions are recruited to the memory trace by BLA memory neurons.

(C) Simultaneous CREB expression in BLA (RG-CREB) and IC (vCREB) enhanced memory in comparison to the control group (EGFP in IC; n = 7–8).

(D) Increased connectivity between vCREB and RG-CREB neurons across brain regions. Comparison of BLA-projecting IC vCREB neurons (rabies/EGFP-positive). More rabies-positive vCREB IC neurons (mm^{-2}) in the CREB group, in comparison to control group (t test) and to chance levels (Fisher's exact test, ****p < 0.0001).

Scale bars, 100 μm (20 μm insets, A and B). t test, *p < 0.05, mean ± SEM.

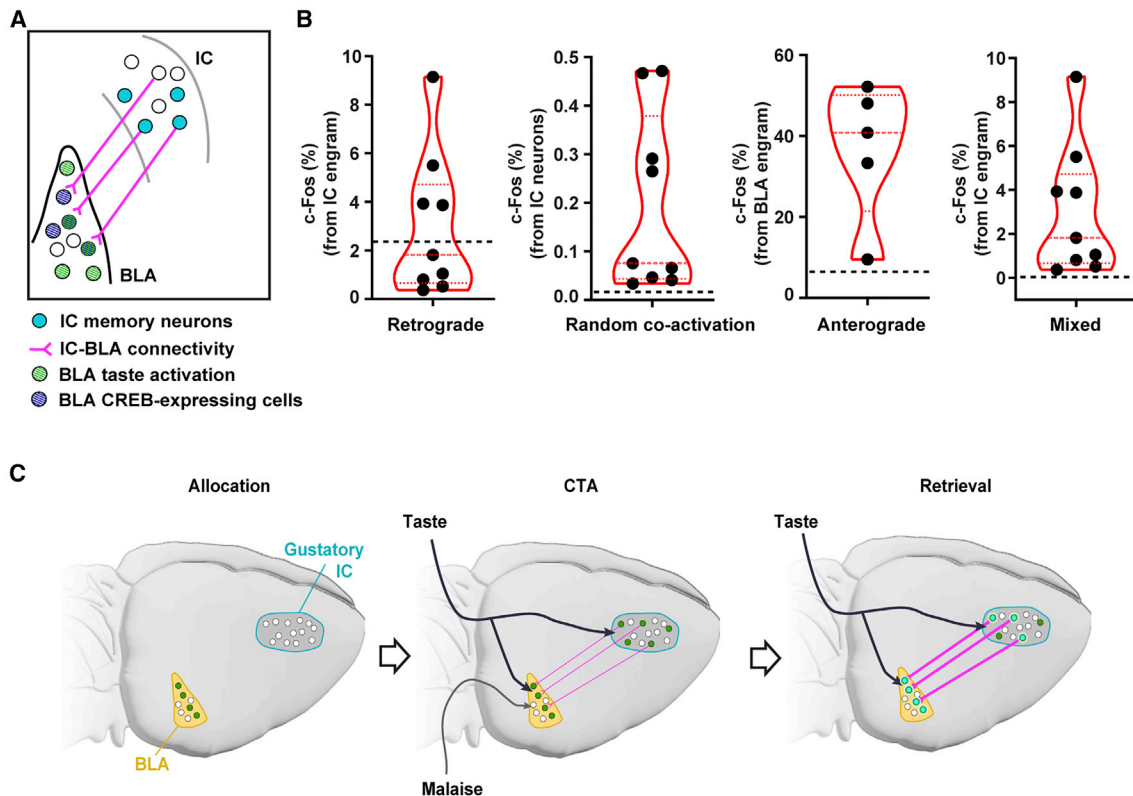


Figure 4. Retrograde model underlying cross-regional coordination of memory allocation

(A) Statistical model for cross-regional coordination of memory allocation.

(B) Comparison of four models' predictions (black dashed line) to experimental results (dashed and dotted red lines indicate median, Q1, and Q3). Predicted activation of IC neurons in the retrograde model (2.22%) fits experimental findings from RG-CREB-projecting IC memory ensembles (3%). Predictions from the random co-activation model (chance activation of connected neurons in both regions), the anterograde model (IC memory neurons choose BLA memory neurons) and the mixed model (IC memory neuron formed by monosynaptic bidirectional connectivity with BLA memory neurons) underestimate observed experimental findings.

(C) A new model for memory ensemble recruitment across brain regions.

DISCUSSION

Here, we demonstrate that the recruitment of neurons to encode a given memory is coordinated across brain regions. Using the CRANE system to tag and trace the connectivity of memory networks in the brain, we showed that memory allocation in one brain region directly recruits presynaptic partners in other brain regions to participate in memory retrieval. We have demonstrated this mechanism between two pairs of bidirectionally connected regions, IC and BLA during CTA (Figure 1) and between BLA and AuCtx during AFC (Figure 2). These results suggest existence of a general retrograde mechanism that coordinates memory formation across different brain regions in a task-specific manner.

Computational models suggest that having a retrograde mechanism that coordinates changes in connectivity between units is essential for information storage and the formation of complex representations.^{38–40} CREB has been shown to regulate pathways of transsynaptic retrograde signaling^{41,42} and thus local allocation induced by RG-CREB might initiate selective strengthening of relevant inputs during learning^{43,44} and

retrogradely transmit this information to presynaptic neurons, recruiting them to the memory trace. In this way, upstream regions benefit from receiving information about plasticity changes occurring in downstream areas.⁴⁵ Comparing CTA with AFC, BLA neurons receiving IC projections might be preferably selected for CTA memory. A recent study suggested CTA memory formation depended on the activity of reciprocally connected excitatory neurons in the IC and BLA,⁴⁶ raising the possibility that an anterograde mechanism might also contribute to the coordination of memory ensembles across brain regions. Although we cannot completely rule out this possibility, our findings and statistical modeling (Figure 4) of both anterograde mechanism, retrograde mechanism, and a mixed model suggest that the retrograde recruitment best explains the mechanism for this coordination.

Finally, we observed an enhancement of memory retrieval, when more memory ensembles were connected between the IC and the BLA (Figure 3), suggesting a direct functional role for the connections between cross-regional memory neurons. This observation can have implications for human memory formation in health and disease, since cross-regional

coordination of neuronal activity is often disrupted in multiple psychiatric disorders that present memory disfunction.^{47,48} Altogether, the results reported here demonstrate that despite the anterograde flow of information between brain regions, there is a retrograde mechanism that shapes the recruitment of memory ensembles in different brain regions to optimize learning and create interconnected, brain-wide memory traces.

STAR★METHODS

Detailed methods are provided in the online version of this paper and include the following:

- **KEY RESOURCES TABLE**
- **RESOURCE AVAILABILITY**
 - Lead contact
 - Materials availability
 - Data and code availability
- **EXPERIMENTAL MODEL AND SUBJECT DETAILS**
 - Animals
- **METHOD DETAILS**
 - Viral constructs
 - CRANE system
 - Surgery and virus infusion
 - Conditioned taste aversion
 - Auditory fear conditioning
 - Tissue processing and immunostaining
 - Whole-brain analysis
 - Model construction and parameters
- **QUANTIFICATION AND STATISTICAL ANALYSIS**

SUPPLEMENTAL INFORMATION

Supplemental information can be found online at <https://doi.org/10.1016/j.neuron.2022.11.018>.

ACKNOWLEDGMENTS

We thank A. Chien, D. Vuong, and M. Feng for technical support, Y. Shen for help with the APV experiment, A. Chowdhury for comments on the manuscript, as well as other members of the Silva laboratory for advice, technical support, and discussions. This work was supported by grants from the NIMH (R01 MH113071), NIA (R01 AG013622), and from the Dr. Miriam and Sheldon G. Adelson Medical Research Foundation to A.J.S.

AUTHOR CONTRIBUTIONS

Conceptualization, A. Lavi and A.J.S.; methodology, A. Lavi; software, A. Lavi; investigation, A. Lavi, M.S., A.F.d.S., A. Luchetti, F.S., D.T.-M., A.O., and C.B.; writing – original draft, A. Lavi, A.F.d.S., M.S., and A.J.S.; supervision, A.J.S.; funding acquisition, A.J.S.

DECLARATION OF INTERESTS

The authors declare no competing interests.

Received: April 4, 2022

Revised: September 29, 2022

Accepted: November 28, 2022

Published: December 22, 2022

REFERENCES

1. DeNardo, L.A., Liu, C.D., Allen, W.E., Adams, E.L., Friedmann, D., Dadgar-Kiani, E., Fu, L., Guenther, C.J., Lee, J.H., Tessier-Lavigne, M., and Luo, L. (2018). Temporal evolution of cortical ensembles promoting remote memory retrieval. *Nat. Neurosci.* 22, 460–469. <https://doi.org/10.1101/295238>.
2. Vousden, D.A., Epp, J., Okuno, H., Nieman, B.J., van Eede, M., Dazai, J., Ragan, T., Bito, H., Frankland, P.W., Lerch, J.P., and Henkelman, R.M. (2014). Whole-brain mapping of behaviourally induced neural activation in mice. *Brain Struct Funct.* 220, 2043–2057. <https://doi.org/10.1007/s00429-014-0774-0>.
3. Josselyn, S.A., and Tonegawa, S. (2020). Memory engrams: recalling the past and imagining the future. *Science* 367, eaaw4325. <https://doi.org/10.1126/science.aaw4325>.
4. Choi, D.I., Kim, J., Lee, H., Kim, J.I., Sung, Y., Choi, J.E., Venkat, S.J., Park, P., Jung, H., and Kaang, B.K. (2021). Synaptic correlates of associative fear memory in the lateral amygdala. *Neuron* 109, 2717–2726.e3. <https://doi.org/10.1016/j.neuron.2021.07.003>.
5. Ryan, T.J., Roy, D.S., Pignatelli, M., Arons, A., and Tonegawa, S. (2015). Engram cells retain memory under retrograde amnesia. *Science* 348, 1007–1013.
6. Han, J.H., Kushner, S.A., Yiu, A.P., Hsiang, H.L., Buch, T., Waisman, A., Bontempi, B., Neve, R.L., Frankland, P.W., and Josselyn, S.A. (2009). Selective erasure of a fear memory. *Science* 323, 1492–1496. <https://doi.org/10.1126/science.1164139>.
7. Zhou, Y., Won, J., Karlsson, M.G., Zhou, M., Rogerson, T., Balaji, J., Neve, R., Poirazi, P., and Silva, A.J. (2009). CREB regulates excitability and the allocation of memory to subsets of neurons in the amygdala. *Nat. Neurosci.* 12, 1438–1443.
8. Han, J.H., Kushner, S.A., Yiu, A.P., Cole, C.J., Matynia, A., Brown, R.A., Neve, R.L., Guzowski, J.F., Silva, A.J., and Josselyn, S.A. (2007). Neuronal competition and selection during memory formation. *Science* 316, 457–460. <https://doi.org/10.1126/science.1139438>.
9. Sano, Y., Shobe, J.L., Zhou, M., Huang, S., Shuman, T., Cai, D.J., Golshani, P., Kamata, M., and Silva, A.J. (2014). CREB regulates memory allocation in the insular cortex. *Curr. Biol.* 24, 2833–2837.
10. Park, S., Kramer, E.E., Mercaldo, V., Rashid, A.J., Insel, N., Frankland, P.W., and Josselyn, S.A. (2016). Neuronal allocation to a hippocampal engram. *Neuropsychopharmacology* 41, 2987–2993. <https://doi.org/10.1038/npp.2016.73>.
11. Arieli, E., Gerbi, R., Shein-Idelson, M., and Moran, A. (2020). Temporally-precise basolateral amygdala activation is required for the formation of taste memories in gustatory cortex. *J. Physiol.* 598, 5505–5522.
12. Piette, C.E., Baez-Santiago, M.A., Reid, E.E., Katz, D.B., and Moran, A. (2012). Inactivation of basolateral amygdala specifically eliminates palatability-related information in cortical sensory responses. *J. Neurosci.* 32, 9981–9991.
13. Hintiryan, H., Bowman, I., Johnson, D.L., Korobkova, L., Zhu, M., Khanjani, N., Gou, L., Gao, L., Yamashita, S., Bienkowski, M.S., et al. (2021). Connectivity characterization of the mouse basolateral amygdalar complex. *Nat. Commun.* 12, 2859. <https://doi.org/10.1038/s41467-021-22915-5>.
14. McDonald, A.J. (1998). Cortical pathways to the mammalian amygdala. *Prog. Neurobiol.* 55, 257–332.
15. Jeong, M., Kim, Y., Kim, J., Ferrante, D.D., Mitra, P.P., Osten, P., and Kim, D. (2016). Comparative three-dimensional connectome map of motor cortical projections in the mouse brain. *Sci. Rep.* 6, 20072. <https://doi.org/10.1038/srep20072>.
16. Doron, G., and Rosenblum, K. (2010). c-Fos Expression Is Elevated in GABAergic Interneurons of the Gustatory Cortex Following Novel Taste Learning. *Neurobiol Learn Mem (Academic Press)*.

17. Adaikkan, C., and Rosenblum, K. (2015). A molecular mechanism underlying gustatory memory trace for an association in the insular cortex. *Elife* 4, e07582.
18. Gogolla, N. (2017). The insular cortex. *Curr. Biol.* 27, R580–R586. <https://doi.org/10.1016/j.cub.2017.05.010>.
19. Bermúdez-Rattoni, F. (2004). Molecular mechanisms of taste-recognition memory. *Nat. Rev. Neurosci.* 5, 209–217. <https://doi.org/10.1038/nrn1344>.
20. Beier, K.T., Kim, C.K., Hoerbelt, P., Hung, L.W., Heifets, B.D., DeLoach, K.E., Mosca, T.J., Neuner, S., Deisseroth, K., Luo, L., and Malenka, R.C. (2017). Rabies screen reveals GPe control of cocaine-triggered plasticity. *Nature* 549, 345–350. <https://doi.org/10.1038/nature23888>.
21. Rogers, A., and Beier, K.T. (2021). Can transsynaptic viral strategies be used to reveal functional aspects of neural circuitry? *J. Neurosci. Methods* 348, 109005. <https://doi.org/10.1016/j.jneumeth.2020.109005>.
22. Stehberg, R.M.-A., and Jimmy. (2012). The Insular Cortex and the Amygdala: Shared Functions and Interactions (IntechOpen). <https://doi.org/10.5772/48495>.
23. Gehrlach, D.A., Weiland, C., Gaitanos, T.N., Cho, E., Klein, A.S., Hennrich, A.A., Conzelmann, K.K., and Gogolla, N. (2020). A whole-brain connectivity map of mouse insular cortex. *eLife* 9, e55585.
24. Escobar, M.L., and Bermúdez-Rattoni, F. (2000). Long-term potentiation in the insular cortex enhances conditioned taste aversion retention. *Brain Res.* 852, 208–212.
25. Kayyal, H., Yiannakas, A., Kolatt Chandran, S.K., Khamsaiy, M., Sharma, V., and Rosenblum, K. (2019). Activity of insula to basolateral amygdala projecting neurons is necessary and sufficient for taste valence representation. *J. Neurosci.* 39, 9369–9382. <https://doi.org/10.1523/JNEUROSCI.0752-19.2019>.
26. Yang, Y., Liu, D.Q., Huang, W., Deng, J., Sun, Y., Zuo, Y., and Poo, M.M. (2016). Selective synaptic remodeling of amygdalocortical connections associated with fear memory. *Nat. Neurosci.* 19, 1348–1355.
27. Winer, J.A., and Lee, C.C. (2007). The distributed auditory cortex. *Hear. Res.* 229, 3–13. <https://doi.org/10.1016/j.heares.2007.01.017>.
28. Fu, J.Y., Yu, X.D., Zhu, Y., Xie, S.Z., Tang, M.Y., Yu, B., and Li, X.M. (2020). Whole-brain map of long-range monosynaptic inputs to different cell types in the amygdala of the mouse. *Neurosci. Bull.* 36, 1381–1394. <https://doi.org/10.1007/s12264-020-00545-z>.
29. Kanold, P.O., Nelken, I., and Polley, D.B. (2014). Local versus global scales of organization in auditory cortex. *Trends Neurosci.* 37, 502–510.
30. Tsukano, H., Horie, M., Ohga, S., Takahashi, K., Kubota, Y., Hishida, R., Takebayashi, H., and Shibuki, K. (2017). Reconsidering tonotopic maps in the auditory cortex and lemniscal auditory Thalamus in mice (frontiers). *Frontiers Neural Circuits* 11, 14. <https://doi.org/10.3389/fncir.2017.00014>.
31. Fürth, D., Vaissière, T., Tzortzi, O., Xuan, Y., Martin, A., Lazaridis, I., Spigolon, G., Fisone, G., Tomer, R., Deisseroth, K., et al. (2018). An interactive framework for whole-brain maps at cellular resolution. *Nat. Neurosci.* 21, 139–149. <https://doi.org/10.1038/s41593-017-0027-7>.
32. Sawatari, H., Tanaka, Y., Takemoto, M., Nishimura, M., Hasegawa, K., Saitoh, K., and Song, W.-J. (2011). Identification and characterization of an insular auditory field in mice. *Eur. J. Neurosci.* 34, 1944–1952. <https://doi.org/10.1111/j.1460-9568.2011.07926.x>.
33. Casanova, J.P., Aguilar-Rivera, M., Rodríguez, M.L.Á., Coleman, T.P., and Torrealba, F. (2018). The activity of discrete sets of neurons in the posterior insula correlates with the behavioral expression and extinction of conditioned fear. *J. Neurophysiol.* 120, 1906–1913. <https://doi.org/10.1152/jn.00318.2018>.
34. Rodríguez, M., Ceric, F., Murgas, P., Harland, B., Torrealba, F., and Contreras, M. (2019). Interoceptive insular cortex mediates both innate fear and contextual threat conditioning to predator odor. *Front. Behav. Neurosci.* 13, 283. <https://doi.org/10.3389/fnbeh.2019.00283>.
35. Casanova, J.P., Madrid, C., Contreras, M., Rodríguez, M., Vasquez, M., and Torrealba, F. (2016). A role for the interoceptive insular cortex in the consolidation of learned fear. *Behav. Brain Res.* 296, 70–77. <https://doi.org/10.1016/j.bbr.2015.08.032>.
36. Ferbinteanu, J. (2019). Memory systems 2018 - Towards a new paradigm. *Neurobiol. Learn. Mem.* 157, 61–78. <https://doi.org/10.1016/j.nlm.2018.11.005>.
37. White, N.M., and McDonald, R.J. (2002). Multiple parallel memory systems in the brain of the rat. *Neurobiol. Learn. Mem.* 77, 125–184. <https://doi.org/10.1006/nlme.2001.4008>.
38. Rumelhart, D.E., Hinton, G.E., and Williams, R.J. (1986). Learning representations by back-propagating errors. *Nature* 323, 533–536. <https://doi.org/10.1038/323533a0>.
39. Whittington, J.C.R., and Bogacz, R. (2019). Theories of error back-propagation in the brain. *Trends Cogn. Sci.* 23, 235–250. <https://doi.org/10.1016/j.tics.2018.12.005>.
40. Jeong, Y., Cho, H.-Y., Kim, M., Oh, J.-P., Kang, M.S., Yoo, M., Lee, H.-S., and Han, J.-H. (2021). Synaptic plasticity-dependent competition rule influences memory formation. *Nat. Commun.* 12, 3915. <https://doi.org/10.1038/s41467-021-24269-4>.
41. Sasaki, M., Gonzalez-Zulueta, M., Huang, H., Herring, W.J., Ahn, S., Ginty, D.D., Dawson, V.L., and Dawson, T.M. (2000). Dynamic regulation of neuronal NO synthase transcription by calcium influx through a CREB family transcription factor-dependent mechanism. *Proc. Natl. Acad. Sci.* 97, 8617–8622.
42. Esvald, E.E., Tuvikene, J., Sirp, A., Patil, S., Bramham, C.R., and Timmusk, T. (2020). CREB family transcription factors are major mediators of BDNF transcriptional autoregulation in cortical neurons. *J. Neurosci.* 40, 1405–1426. <https://doi.org/10.1523/JNEUROSCI.0367-19.2019>.
43. Sargin, D., Mercaldo, V., Yiu, A.P., Higgs, G., Han, J.H., Frankland, P.W., and Josselyn, S.A. (2013). CREB regulates spine density of lateral amygdala neurons: implications for memory allocation. *Front. Behav. Neurosci.* 7, 209. <https://doi.org/10.3389/fnbeh.2013.00209>.
44. Barco, A., Alarcon, J.M., and Kandel, E.R. (2002). Expression of constitutively active CREB protein facilitates the late phase of long-term potentiation by enhancing synaptic capture. *Cell* 108, 689–703. [https://doi.org/10.1016/s0092-8674\(02\)00657-8](https://doi.org/10.1016/s0092-8674(02)00657-8).
45. Harris, K.D. (2008). Stability of the fittest: organizing learning through retroaxonal signals. *Trends Neurosci.* 31, 130–136. <https://doi.org/10.1016/j.tins.2007.12.002>.
46. Abe, K., Kuroda, M., Narumi, Y., Kobayashi, Y., Itohara, S., Furuichi, T., and Sano, Y. (2020). Cortico-amygdala interaction determines the insular cortical neurons involved in taste memory retrieval. *Mol. Brain* 13, 107. <https://doi.org/10.1186/s13041-020-00646-w>.
47. Woodward, N.D., and Cascio, C.J. (2015). Resting-state functional connectivity in psychiatric disorders. *JAMA Psychiatry* 72, 743–744. <https://doi.org/10.1001/jamapsychiatry.2015.0484>.
48. Fornito, A., Zalesky, A., Pantelis, C., and Bullmore, E.T. (2012). Schizophrenia, neuroimaging and connectomics. *Neuroimage* 62, 2296–2314. <https://doi.org/10.1016/j.neuroimage.2011.12.090>.
49. Zolotukhin, S., Potter, M., Zolotukhin, I., Sakai, Y., Loiler, S., Fraitas, T.J., Jr., Chiodo, V.A., Phillipsberg, T., Muzyczka, N., Hauswirth, W.W., et al. (2002). Production and purification of serotype 1, 2, and 5 recombinant adeno-associated viral vectors. *Methods* 28, 158–167. [https://doi.org/10.1016/s1046-2023\(02\)00220-7](https://doi.org/10.1016/s1046-2023(02)00220-7).
50. Lee, Y.S., Ehninger, D., Zhou, M., Oh, J.Y., Kang, M., Kwak, C., Ryu, H.H., Butz, D., Araki, T., Cai, Y., et al. (2014). Mechanism and treatment for learning and memory deficits in mouse models of Noonan syndrome. *Nat. Neurosci.* 17, 1736–1743. <https://doi.org/10.1038/nn.3863>.
51. Zhou, M., Greenhill, S., Huang, S., Silva, T.K., Sano, Y., Wu, S., Cai, Y., Nagaoka, Y., Sehgal, M., Cai, D.J., et al. (2016). CCR5 is a suppressor for cortical plasticity and hippocampal learning and memory. *eLife* 5, e20985. <https://doi.org/10.7554/eLife.20985>.
52. Kim, E.J., Jacobs, M.W., Ito-Cole, T., and Callaway, E.M. (2016). Improved monosynaptic neural circuit tracing using engineered rabies virus

- glycoproteins. *Cell Rep.* 15, 692–699. <https://doi.org/10.1016/j.celrep.2016.03.067>.
53. Park, A., Jacob, A.D., Walters, B.J., Park, S., Rashid, A.J., Jung, J.H., Lau, J., Woolley, G.A., Frankland, P.W., and Josselyn, S.A. (2019). A time-dependent role for the transcription factor CREB in neuronal allocation to an engram underlying a fear memory revealed by using a novel. *Neuropsychopharmacology* 45, 916–924.
54. Wickersham, I.R., Lyon, D.C., Barnard, R.J., Mori, T., Finke, S., Conzelmann, K.K., Young, J.A., and Callaway, E.M. (2007). Monosynaptic restriction of transsynaptic tracing from single, genetically targeted neurons. *Neuron* 53, 639–647. <https://doi.org/10.1016/j.neuron.2007.01.033>.
55. Lavi, K., Jacobson, G.A., Rosenblum, K., and Lüthi, A. (2018). Encoding of conditioned taste aversion in cortico-amygdala circuits. *Cell Rep.* 24, 278–283.
56. Franklin, K.B.J., and Paxinos, G. (2013). *Paxinos and Franklin's The Mouse Brain in Stereotaxic Coordinates, Fourth Edition* (Academic Press).
57. Oh, S.W., Harris, J.A., Ng, L., Winslow, B., Cain, N., Mihalas, S., Wang, Q., Lau, C., Kuan, L., Henry, A.M., et al. (2014). A mesoscale connectome of the mouse brain. *Nature* 508, 207–214. <https://doi.org/10.1038/nature13186>.
58. Keller, D., Erö, C., and Markram, H. (2018). Cell densities in the mouse brain: A systematic review. *Front. Neuroanat.* 12, 83.
59. Murakami, T.C., Mano, T., Saikawa, S., Horiguchi, S.A., Shigeta, D., Baba, K., Sekiya, H., Shimizu, Y., Tanaka, K.F., Kiyonari, H., et al. (2018). A three-dimensional single-cell-resolution whole-brain atlas using CUBIC-X expansion microscopy and tissue clearing. *Nat. Neurosci.* 21, 625–637. <https://doi.org/10.1038/s41593-018-0109-1>.
60. Tsai, P.S., Kaufhold, J.P., Blinder, P., Friedman, B., Drew, P.J., Karten, H.J., Lyden, P.D., and Kleinfeld, D. (2009). Correlations of neuronal and microvascular densities in murine cortex revealed by direct counting and colocalization of nuclei and vessels. *J. Neurosci.* 29, 14553–14570. <https://doi.org/10.1523/jneurosci.3287-09.2009>.
61. Yasoshima, Y., Scott, T.R., and Yamamoto, T. (2006). Memory-dependent c-Fos expression in the nucleus accumbens and extended amygdala following the expression of a conditioned taste aversive in the rat. *Neuroscience* 141, 35–45. <https://doi.org/10.1016/j.neuroscience.2006.03.019>.
62. Kim, M.J., Mizumori, S.J.Y., and Bernstein, I.L. (2010). Neuronal representation of conditioned taste in the basolateral amygdala of rats. *Neurobiol. Learn. Mem.* 93, 406–414. <https://doi.org/10.1016/j.nlm.2009.12.007>.
63. Yasoshima, Y., Shimura, T., and Yamamoto, T. (1995). Single unit responses of the amygdala after conditioned taste aversion in conscious rats. *Neuroreport* 6, 2424–2428.
64. Grossman, S.E., Fontanini, A., Wieskopf, J.S., and Katz, D.B. (2008). Learning-related plasticity of temporal coding in simultaneously recorded amygdala-cortical ensembles. *J. Neurosci.* 28, 2864–2873. <https://doi.org/10.1523/JNEUROSCI.4063-07.2008>.
65. Fontanini, A., Grossman, S.E., Figueroa, J.A., and Katz, D.B. (2009). Distinct subtypes of basolateral amygdala taste neurons reflect palatability and reward. *J. Neurosci.* 29, 2486–2495.
66. Fletcher, M.L., Ogg, M.C., Lu, L., Ogg, R.J., and Boughter, J.D., Jr. (2017). Overlapping representation of primary tastes in a defined region of the gustatory cortex. *J. Neurosci.* 37, 7595–7605.
67. Katz, D.B., Simon, S.A., and Nicolelis, M.A. (2001). Dynamic and multimodal responses of gustatory cortical neurons in awake rats. *J. Neurosci.* 21, 4478–4489.
68. Levitan, D., Lin, J.Y., Wachutka, J., Mukherjee, N., Nelson, S.B., and Katz, D.B. (2019). Single and population coding of taste in the gustatory cortex of awake mice. *J. Neurophysiol.* 122, 1342–1356. <https://doi.org/10.1152/jn.00357.2019>.
69. Moran, A., and Katz, D.B. (2014). Sensory cortical population dynamics uniquely track behavior across learning and extinction. *J. Neurosci.* 34, 1248–1257. <https://doi.org/10.1523/JNEUROSCI.3331-13.2014>.
70. Faul, F., Erdfelder, E., Lang, A.G., and Buchner, A. (2007). G*Power 3: a flexible statistical power analysis program for the social, behavioral, and biomedical sciences. *Behav. Res. Methods* 39, 175–191. <https://doi.org/10.3758/bf03193146>.

STAR★METHODS

KEY RESOURCES TABLE

| REAGENT or RESOURCE | SOURCE | IDENTIFIER |
|--|---|--|
| Antibodies | | |
| Anti-cFos (rabbit) | Cell Signalling | Cat#2250; RRID: AB_2247211 |
| Alexa647 goat anti-rabbit | Invitrogen | Cat#A-21245; RRID: AB_2535813 |
| Streptavidin Protein, DyLight™ 488 | ThermoFisher | Cat#21832 |
| DAPI | Life Technologies | Cat#D-21490 |
| ProLong Gold antifade mounting media | Life Technologies | Cat#P36934 |
| Avidin/Biotin Blocking Kit | Vector Laboratories | Cat#SP-2001 |
| Biotin anti-HA | BioLegend | Cat#BIOT-101L; RRID: AB_2565023 |
| Bacterial and virus strains | | |
| pAAVhSyn-CpBG-2A-HA-CREB ('RG') | Prepared and purified ^{49–51} | N/A |
| pAAV-hSyn-TVA ('TVA') | Prepared and purified ^{49–51} | N/A |
| pAAV-hSyn-hChr2(H134R)-EYFP | Chan et al., Nat Neurosci, 20(8):1172–1179. | RRID:Addgene_26973 |
| pDire | Osterwalder et al., Nat Methods, 7(11):893–5. | RRID:Addgene_26745 |
| mCerulean-N1 | Rizzo et al., Nat Biotechnol. 22(4):445–9. | RRID:Addgene_54758 |
| pAAV-hSyn-iCRE-2A-HA-CREB | Subcloned | N/A |
| pAAV-hSyn-CpBG-2A-HA-Cerulean | Subcloned | N/A |
| pAAV-hSyn-iCRE-2A-HA-Cerulean | Subcloned | N/A |
| Rabies-EnvA(PBG)ΔG-mCherry | Salk Viral Vector | N/A |
| Chemicals, peptides, and recombinant proteins | | |
| Super-glue | Loctite | Cat#45198 |
| Dental Cement | Lang Dental | Cat#1223CLR |
| D-APV | Sigma | Cat#A8054 |
| Lithium Chloride | Sigma | Cat#L4408 |
| Saccharin | Sigma | Cat#109185 |
| Deposited data | | |
| Raw data of quantifications | This paper Main and supplemental figures | N/A |
| Experimental models: Organisms/strains | | |
| Adult F1 hybrid | Taconic Farms | C57Bl/6NTac × 129S6/SvEvTac |
| Software and algorithms | | |
| R | R Foundation for Statistical Computing | RRID:SCR_001905 |
| Automated Freezing | Med Associates INC (Video Freeze®) Software) | RRID:SCR_014574 |
| Prism 9.0.2 | GraphPad Software, La Jolla | RRID:SCR_002798 |
| NIS-Elements AR 5.02.00 | Nikon | RRID:SCR_014329 |
| WholeBrain | Furth et al., Nat Neurosci, 21(1):139–149. | https://github.com/tractatus/wholebrain |
| Whole-brain analysis | This paper | https://doi.org/10.5281/zenodo.7352497 , https://github.com/laviayal/wholebrain-analysis |
| Other | | |
| Nanoject II | Fisher Scientific | Cat#13 681 455 |
| Nanoject Controller | World Precision Instrument | Cat#SYS-MICRO4 |
| Guide Cannula | Plastics One | Cat#C313GS-5/SPC |
| Internal Cannula | Plastics One | Cat#C313IS-5/SPC |

RESOURCE AVAILABILITY

Lead contact

Further information and requests for resources should be directed to and will be fulfilled by the lead contact, Alcino J Silva (silvaa@mednet.ucla.edu).

Materials availability

All unique/stable reagents generated in this study are available from the [lead contact](#) upon request with a completed Materials Transfer Agreement.

Data and code availability

- Data reported in this paper are available from the [lead contact](#) upon reasonable request.
- All original code has been deposited at Zenodo and is publicly available. DOI and a link to the code in the GitHub repository are listed in the [key resources table](#).
- Any additional information required to reanalyze the data reported in this paper is available from the [lead contact](#) upon request.

EXPERIMENTAL MODEL AND SUBJECT DETAILS

Animals

Adult F1 hybrid (C57Bl/6NTac × 129S6/SvEvTac) male mice 3 to 5 months old were used in behavioral analyses. Mice were group housed with free access to food and water, and maintained on a 12:12 hour light:dark cycle. All experiments were performed during the light phase of the cycle. All studies were approved by the Animal Research Committee at UCLA.

METHOD DETAILS

Viral constructs

For the CRANE AAV system, Recombinant virus (rAAV5) for all plasmids, including pAAV-hSyn-CpBG-2A-HA-CREB ('RG') and pAAV-hSyn-TVA ('TVA') were prepared and purified as previously described.^{49–51} All AAV constructs were subcloned into pAAV-hSyn-hChR2(H134R)-EYFP; pAAV-hSyn-hChR2(H134R)-EYFP was a gift from Karl Deisseroth (Addgene plasmid #26973; <http://n2t.net/addgene:26973>; RRID:Addgene_26973). For the Rabies helper viruses, we used CpBG as the Rabies G-protein helper. CpBG and TVA were a gift from Dr. Edward Callaway,⁵² and were sub-cloned together with the full-length CREB gene.⁹ For the pAAV-hSyn-iCRE-2A-HA-CREB, we subcloned iCRE from pDIRE into pAAV-hSyn-CpBG-2A-HA-CREB. pDIRE was a gift from Rolf Zeller (Addgene plasmid #26745; <http://n2t.net/addgene:26745>; RRID:Addgene_26745). For control experiments, Cerulean fluorescent protein (CFP) was subcloned from mCerulean-N1 into the respective constructs generating, pAAV-hSyn-CpBG-2A-HA-Cerulean and pAAV-hSyn-iCRE-2A-HA-Cerulean. mCerulean-N1 was a gift from Michael Davidson & Dave Piston (Addgene plasmid #54758; <http://n2t.net/addgene:54758>; RRID:Addgene_54758) Recombinant virus (rAAV5) was purified. Vector titers were determined by Real Time PCR. All titers for AAV viruses were above 1.6×10^{12} genome copies/ml and were matched between CREB and control groups.

CRANE system

The CRANE system uses a combination of three viruses. The first virus carries the CREB gene, which biases memory allocation to a sparse and random subset of neurons in a given brain region.^{7,8,53} The CREB virus also encodes a rabies glycoprotein (RG, separated by a T2A endonuclease) which is critical for rabies retrograde transsynaptic tracing.⁵⁴ As a control, we used a virus that labeled a random population of cells by substituting CREB with the cerulean fluorescent protein (CFP; RG-CFP). The second virus (AAV-TVA) encodes TVA, a cell membrane protein that is essential for rabies infection.⁵⁴ Consequently, only cells expressing both RG-2A-CREB (or CFP) and TVA are capable of retrograde tracing with the rabies virus Rabies- Δ G-mCherry(EnvA), the third virus in the CRANE system. This rabies virus, which also expresses mCherry, spreads to only one synapse retrogradely, since presynaptic neurons do not express the rabies G-protein.⁵⁴ RG-CREB and Wt mice showed comparable learning levels. The percent of rabies-positive cells is in line with expected overall connectivity between IC and BLA^{55,25,46}

Surgery and virus infusion

Mice were anaesthetized with 1.5 to 2.0% isoflurane for surgical procedures and placed into a stereotactic frame (model #1900, David Kopf Instruments, Tujunga, CA) on a heating pad. Artificial tears were applied to the eyes to prevent drying. Subcutaneous saline injections were administered throughout each surgical procedure to prevent dehydration. In addition, carprofen (5 mg kg⁻¹) and dexamethasone (0.2 mg kg⁻¹) were administered both during surgery and for 2-7 days post-surgery. A midline incision was made down the scalp, and we used the stereotaxic drilling unit (model 1911, David Kopf Instruments, Tujunga, CA) to perform craniotomy. After cannula implantation, mice were single-housed. Water with amoxicillin was administered for two weeks. For virus

injection, a Nanoliter injector (World Precision Instruments) was used to infuse virus with Micro4 Controller (World Precision Instruments). Virus was infused at 50 nL/min. After infusion, the capillary was kept at the injection site for 5 min and then withdrawn slowly. For rabies tracing, 300 nl of 3:7 volume mixture of pAAV-hSyn-CpBG-2A-HA-CREB (or pAAV-hSyn-CpBG-2A-HA-Cerulean as control) and pAAV-hSyn-TVA was injected into the BLA or IC. For the dual-CREB experiment, 300nl of 1:1 volume mixture of pAAV-hSyn-iCRE-2A-HA-CREB (or pAAV-hSyn-iCRE-2A-HA-Cerulean as control) and AAV8-FLEX-EGFP was injected into the IC. Following virus injection for rabies tracing, stainless steel cannulas were implanted to improve recovery time from the virus infusion and reduce recurrent damage to the tissue. Bilateral guide cannulas (Plastics One, C313GS-5/SPC) were implanted and fixed on the skull with dental cement. After cannula implantation, mice were single-housed. Four days before the CTA protocol (6 days for AFC), mice were anesthetized and Rabies-EnvA(PBG) Δ G-mCherry (Salk Viral Vector core titer 1.0×10^8 ; 0.8 μ L, 100nL/min) was infused through the internal cannula (Plastics One, C313IS-5/Spc) at the helper viruses injection coordinates. After infusion, the internal cannula was left in place for an additional 8 min to ensure full diffusion. For APV experiments, Saline or D-APV (Sigma, A8054 10 μ g/ μ L in Saline; 0.4 μ L, 100nL/min) were bilaterally infused through the same BLA internal cannula as above that were left for an additional 5 minutes. Coordinates used were taken from the mouse brain atlas⁵⁶ (relative to Bregma, midline, or dorsal brain surface and in mm): BLA: AP -1.3, ML \pm 3.3, DV -4.8; IC: AP +0.7, ML \pm 3.55, DV -2.8 and AP +0.2, ML \pm 3.7, DV -3.0.

Conditioned taste aversion

The conditioned taste aversion task was carried out as previously described^{7,16,17} with minor modifications. CTA training took place 2 weeks following surgery, in the light part of the cycle. Four days after infusion of the rabies virus into the BLA or IC, mice started the CTA behavioral protocol. Mice were water deprived for 24 h and then habituated to the training cage for 3 days to get their daily water ration within 30 min per day from two tubes (10 ml each). Habituation started 4 days after rabies virus infusion. On the conditioning day, the two tubes were filled with 0.2% saccharin sodium salt (w/v, the taste CS) instead of water. The CS was presented for 30 min and 20 min later, mice were treated with the malaise inducing agent lithium chloride (LiCl; 0.15 M, 2% body weight i.p.). Testing for aversion to saccharin occurred 3 days later. Two tubes (containing saccharin) were presented for 30 min. The intake of each fluid was measured and the learning index (LI) was defined as follows: [(milliliters consumed during training)/(milliliters during training + milliliters during retrieval)] \times 100%. For APV experiments, Saline or APV were infused 30 minutes prior to training. LI was defined as the ratio between Saccharin and water in the prior day as follows: [(milliliters consumed a day before retrieval)/(milliliters consumed a day before retrieval + milliliters during retrieval)] \times 100%. The ratio between Saccharin and water in the prior day was similar between groups before training, and was significantly lower in the APV group at retrieval ($n=5-6$, t-test, $P<0.05$) where it was at chance levels (t-test, $P=0.74$). For the dual-CREB experiment, we used 0.1% saccharin to uncover changes in LI and avoid ceiling effects. For this experiment LI was calculated: [(milliliters of water consumed)/(milliliters of water + milliliters of saccharin consumed)] \times 100%. 50% LI is equal preference level, and the higher the LI, the less mice preferred saccharin). We confirmed that both LIs were correlated (Pearson correlation; $R^2 = 0.961$, $P < 0.0001$).

Auditory fear conditioning

Auditory fear conditioning was carried out as previously described⁷ with minor modifications. Training consisted of placing the mice in a conditioning chamber, and 2 min later presenting a series of 10 tones, 14kHz each at 85dB, co-terminating with a 2-sec electric foot shock (0.5mA) through the floor grid. This was repeated 5 times at pseudo-random intervals (30 to 60 sec). Afterwards the mice remained in the chamber for an additional 2 min. Test for auditory fear conditioning occurred 3 days later. Mice were placed in a novel chamber (Context B) and 2 min later the tone CS was presented (for 1 min). Our index of memory, freezing (the cessation of all movement except for respiration), was assessed via an automated scoring system (Med Associates Inc.) with a 30 frames/sec sampling; the mice needed to freeze continuously for at least 1 sec before freezing was counted.

Tissue processing and immunostaining

Mice were transcardially perfused 90 minutes following behavioral retrieval with 4% PFA (4% paraformaldehyde in 0.1 M phosphate buffer), and after perfusion brains were extracted and incubated with 4% PFA overnight at 4°C. Coronal sections were cut at 50 μ m on a microtome and transferred to PBS, then blocked in 5% Normal Goat Serum in 0.1 M PBS and 0.1% TritonX-100 for 1 hr. Immunostaining for HA staining was used to identify the expression of RG-CREB or RG-CFP in the tissue. For biotin-conjugated primary antibodies, slices were additionally blocked with Avidin/Biotin Blocking Kit (Vector Laboratories, #SP-2001). After blocking, sections were incubated in a primary antibody mix (in 0.1 M PBS, 0.2% TritonX-100 and 5% Normal Goat Serum) of rabbit anti-c-Fos (Cell Signaling, #2250, 1:700) or biotin anti-HA (BioLegend, # BIOT-101L, 1:100) for two days at 4°C. After 3 \times 15 min washes in 0.1 M PBS and 0.2% TritonX-100 the secondary antibodies (1:1000 dilution) were applied (in 0.1 M PBS, 0.2% TritonX-100 and 3% Normal Goat Serum): Alexa647 goat anti-rabbit (Invitrogen #A-21245) or Streptavidin Protein, DyLight™ 488 (ThermoFisher #21832). Slices were incubated in the secondary mix for 2 hr at room temperature. After 2 \times 15 min washes in 0.1 M PBS and 0.1% TritonX-100, slices were incubated with 4',6-diaminodino-2-phenylindole (DAPI, Life Technologies D-21490, 1:2000) for 15 min, and then were further washed with 0.1 M PBS and 0.1% TritonX-100 for 15 min before mounted onto slides with ProLong Gold antifade mounting media (Life Technologies, P36934). At least 3 slices from each experiment were incubated without the primary antibody to control for its binding specificity. All immunostaining images were acquired with a Nikon A1 Laser Scanning Confocal Microscope (LSCM). Whole-slice images were obtained by tiling 4x images. Analysis was performed on 20x Z-stack images.

For quantification of c-Fos and mCherry (for Rabies), we used the Nikon Elements 3D counting module. All counts and co-localizations of c-Fos and rabies were verified manually by an expert blinded to image identity. For Figure 2H, heatmap was generated base on localization of cells that were both rabies positive and c-Fos positive in the Allen Mouse Common Coordinate Framework brain atlas.⁵⁷ To control for the variability in rabies and c-Fos expression between mice, we calculated chance levels for each mouse. To normalize for chance, we subtracted chance (rabies/DAPI) × (c-Fos/DAPI) × 100 from the observed overlap (rabies and c-Fos)/DAPI × 100 and then divided by chance. To calculate the Network activation index (NAI; Figure S5C), chance levels were calculated for rabies (*chanceRabies*) and EGFP (*chanceEGFP*). Then, the difference-sum ratio was calculated DR = (chanceRabies - *chanceEGFP*)/(chanceRabies + *chanceEGFP*+2) and scaled to an index between 0 and 1 NAI = (DR+1)/2.

Whole-brain analysis

Brain slice images were aligned automatically to the corresponding Bregma, based on the Allen brain atlas. Then, brain maps were fine-tuned manually by an expert, blinded to the experimental condition, based on anatomic landmarks in an unbiased manner. Next, previous cell count data that were obtained from Z-stack analyses were overlaid on the Allen brain atlas using the WholeBrain platform³¹ and a custom-made R script (script available upon request).

Model construction and parameters

We propose 3 models that could account for how memories are formed between directly connected neurons across brain regions. All models assumed that each BLA neuron is innervated by at most one neuron from the IC. We used numbers from the literature, where available. These include the number and proportion of neurons in the BLA and IC,^{58–60} the extent of projections from IC to BLA,^{25,46} c-Fos in the BLA following CTA retrieval,⁶¹ and the extent of neuronal response to taste in the BLA^{62–65} and the IC^{55,66–69} (i.e., how many neurons were activated following exposure of the mice to taste in each respective region). We also confirmed that several experimental numbers we used match measurements from previous studies, such as the percentage of neurons in the IC that are activated upon CTA retrieval⁹ and the percentage of vCREB-expressing neurons in the BLA.^{7,8,43}

The anterograde model

$$\%BLA_{IC} = \frac{\#IC}{\#BLA} \times \frac{\%IC_{taste} \times \% (IC \rightarrow BLA|IC)}{\%BLA_{memory}}$$

The anterograde model simulated the percentage of neurons in the BLA that encode taste and received projections from IC memory neurons out of all BLA memory neurons (%BLA_{IC}). Activation of neurons in the IC, that are directly connected to the BLA, induces the activation of their counterparts in the BLA. Taking into account the ratio between the number of neurons in the IC (#IC) and the number of neurons in the BLA (#BLA), the anterograde model assumes that only BLA neurons that are directly connected by IC neurons participate in memory encoding and its subsequent storage. This model further considers the percentage of taste-activated neurons in the IC (%IC_{taste}) and the connectivity from the IC to the BLA (%IC → BLA|IC), out of the memory neuronal population in the BLA (%BLA_{memory}). The model predicts that the percentage of BLA neurons that encode taste and receive projections from IC memory neurons, out of all the BLA memory neurons, is 6%. Since in our experimental setup, vCREB neurons are the ones connected to the IC (and vCREB is expressed in random cells prior to the CTA), we compared the prediction of this model to the observed percentage of BLA vCREB-expressing neurons that were activated during learning. We found that 36% of the BLA memory neurons were vCREB neurons – 6 times higher than expected. This implies that the anterograde mechanism in of itself would not be sufficient to explain our results in the BLA. (for this model we used the following numbers: #IC = 90,000, #BLA = 194,000, %IC_{taste} = 36%, %IC → BLA|IC = 0.5%, %BLA_{memory} = 1.38%)

The random model

$$\%IC \rightarrow BLA_{taste} = \%BLA_{taste} \times \% (IC \rightarrow BLA|IC) \times \%IC_{taste}$$

The random co-activation model simulates the percentage of IC neurons that encode taste and project to BLA neurons that are also activated by taste (%IC → BLA_{taste}). According to this model, memory allocation in both the BLA and the IC is random and the connection between memory neurons across these brain regions is thus determined by the percentage of taste-responding neurons in the IC (%IC_{taste}) that are connected (%IC → BLA|IC) to taste-responding neurons in the BLA (%BLA_{taste}). This model predicts that the percentage of IC neurons that encode taste and project to BLA neurons, that are also activated by taste, is 0.029%. As with the Anterograde model, we compared the predictions of this model to the observed percentage of IC neurons that connect to vCREB-expressing neurons in the BLA and found that it is 0.2% (almost 7 times higher than what we observed). (for this model we used the following numbers: %IC_{taste} = 36%, %IC → BLA|IC = 0.5%, %BLA_{taste} = 16%)

The retrograde model

$$\%IC_{BLA} = \frac{\#BLA}{\#IC} \times \frac{\%BLA_{taste} \times \% (IC \rightarrow BLA|BLA) \times \%BLA_{CREB}}{\%IC_{memory}}$$

The Retrograde model simulates the percentage of IC neurons that encode taste and project to BLA memory neurons out of all IC memory neurons. In this model, memory neurons in the BLA affect the probability that IC neurons that project to them participate in memory encoding and retrieval. This model considers the probability that vCREB-expressing neurons (%BLA_{CREB}) are activated by taste (%BLA_{taste}) and receive projections from the IC (%IC → BLA|BLA) out of the memory neuronal population in the IC (%IC_{memory}). The model predicts that the % of IC memory neurons that connect to vCREB-expressing BLA memory neurons, out of all of the IC memory neurons, would be 2.22%. Our observations confirm this prediction since we found 3% ± 0.92% of such IC neurons, well within the expected experimental error. (for this model we used the following numbers: #IC = 90,000, #BLA = 194,000, %BLA_{taste} = 16%, %IC → BLA|BLA = 1.71%, %IC_{memory} = 3.6%, %BLA_{CREB} = 13.56%)

The mixed model (anterograde & retrograde)

$$\%IC_{BLA} = \frac{\#BLA}{\#IC} \times \frac{\%BLA_{taste} \times \% (IC \rightarrow BLA|BLA) \times \%BLA_{CREB} \times \% (IC \leftarrow BLA|BLA)}{\%IC_{memory}}$$

Similar to the Retrograde model, the Mixed model simulates %IC_{BLA}, the percentage of IC neurons that encode taste and project to BLA memory neurons out of all IC memory neurons. However, in this model, memory neurons in the BLA affect the probability that IC neurons participate in memory encoding and retrieval, only if they project to them and also receive input from them. Therefore, this model adds (%IC → BLA|BLA) to the other Retrograde parameters, which accounts for the projections from the BLA to the IC. The model predicts that the percentage of IC memory neurons that connect to and receive input from vCREB-expressing BLA memory neurons, out of all of the IC memory neurons, would be 0.0029%. Comparing the predictions to our observations, this model underestimates %IC_{BLA}, suggesting that the low proportion of the IC memory neurons that send and receive input from the BLA is not high enough to explain the experimental observations. (for this model we used the following numbers: #IC = 90,000, #BLA = 194,000, %BLA_{taste} = 16%, %IC → BLA|BLA = 1.71%, %IC → BLA|BLA = 0.13%, %IC_{memory} = 3.6%, %BLA_{CREB} = 13.56%)

QUANTIFICATION AND STATISTICAL ANALYSIS

The investigators who collected and analyzed the data, including behavior and staining, were blinded to treatment conditions. Error bars in the figures indicate the SEM. All statistical analyses were performed using GraphPad Prism 9. N designates the number of mouse or brains collected, unless otherwise stated. Mice with mistargeted virus injections were excluded from analysis. We analyzed at least 4 images per mouse from both left and right hemispheres. Power analyses using G*Power version 3.1.9.7⁷⁰ show at least 80% power for each main finding. Statistical significance was assessed by Student’s two-sided t-test, or one- or two-way ANOVA where appropriate, followed by the indicated post-hoc tests. Evaluating the likelihood of a cell to be recruited above chance level was based on Fisher’s exact test. The level of significance was set at P < 0.05.